# Decagonal quasicrystalline or microcrystalline structures: The specific case of Al-Cu-Co(-Si)

M. Fettweis, P. Launois, F. Dénoyer, R. Reich, and M. Lambert
*Laboratoire de Physique des Solides, Université Paris Sud, Bâtiment 510, 91405 Orsay Cedex, France*
(Received 19 October 1993)

An extensive structural analysis of a decagonal $Al_{63}Cu_{17.5}Co_{17.5}Si_2$ alloy is reported. The structure is analyzed within the context of both microcrystalline and quasicrystalline models through the examination of single-crystal x-ray diffraction patterns. We conclude that our sample is in a microcrystalline state formed of coherent twins of an approximant state of the quasicrystal. We underline that diffraction patterns exhibiting sharp peaks and perfect tenfold symmetry do not necessarily correspond to long-range quasiperiodic order, which could have implications for the physical properties of quasicrystal-like alloys. The present work also gives us the opportunity to point out and discuss some general features: (i) the intensity cutoff problem for quasicrystal structure determinations, (ii) the consequence in structure determination if a sample supposed to be a quasicrystal is in fact a microcrystal, and (iii) the proper determination of basis vectors in decagonal quasicrystals.

## I. INTRODUCTION

Soon after the discovery of an icosahedral quasicrystal in an Al-Mn alloy in 1984,[1] a decagonal quasicrystal formed of periodically stacked quasicrystalline planes exhibiting tenfold symmetry in their diffraction patterns was found in the same alloy in 1985.[2] Numerous quasicrystalline alloys have now been found (see, e.g., Tables 4–6 in Ref. 3). The first quasicrystals were not equilibrium states and had important structural defects. Stable and perfect quasicrystals have been discovered since 1988. This is, particularly, the case of Al-Cu-Co(-Si) alloys. Decagonal $Al_{65}Cu_{20}Co_{15}$ was discovered in 1988 (Ref. 4) and decagonal $Al_{65-x}Cu_{20}Co_{15}Si_x$, substituting a little silicon for aluminium, was discovered in 1990.[5] Extensive structural studies, transport, and mechanical property investigations of Al-Cu-Co(-Si) alloys have been made since these discoveries. Metallurgical studies were carried out, leading to an Al-Cu-Co ternary equilibrium diagram.[6] Decagonal approximants or twins of domains of approximant phases were also found in Al-Cu-Co-Si (see, e.g., Refs. 7–13).

This paper is devoted to the $Al_{63}Cu_{17.5}Co_{17.5}Si_2$ "structure analysis" with the aim of distinguishing between quasicrystalline and microcrystalline structures. It also gives us the opportunity to review and discuss some general features about these models. Section II describes the experimental part in which x-ray single-crystal diffraction patterns are presented. In Sec. III, we first summarize the quasicrystalline model of Steurer and Kuo[14] (SK) and discuss the direct space description. Then we show that our diffraction data cannot be analyzed within the framework of this model. Within this part, we also discuss the reciprocal space intensity cutoff problem for quasicrystal structure determinations. In Sec. IV, after a generic presentation of the microcrystalline model, we describe our data analysis and prove that our sample is in a microcrystalline state formed of coherent twins of an approximant phase of the quasicrystal. In Sec. V, we discuss the problem of choosing the exact atomic decoration in the approximant phase and we raise three general points: (i) the question of the domain arrangement in a microcrystal, (ii) the consequence in structure determination if a sample taken as a quasicrystal is, in fact, a microcrystal, (iii) the proper determination of basis vectors in decagonal quasicrystals. Finally, Sec. VI concludes the paper.

## II. EXPERIMENTAL RESULTS: X-RAY SINGLE-CRYSTAL STUDY OF DECAGONAL $Al_{63}Cu_{17.5}Co_{17.5}Si_2$

### A. Experiments

The growth method which allows one to get decagonal needles in Al-Cu-Co(-Si) alloys is as follows. The first stage consists in a rapid solidification: an alloy of nominal composition $Al_{63}Cu_{17.5}Co_{17.5}Si_2$ and of initial weight 3.7 g is prepared by induction melting of the high-purity elements (99.99%) into a pointed boron nitride crucible under argon atmosphere. In order to homogenize the ingot and to produce very small quasicrystalline-type seeds, the melt is overheated about 100 K above the liquidus temperature. A rapid cooling (by switching off the heating electric high-tension current) produces a porous ingot with a fine peritectic structure (small decagonal grains) embedded in various crystalline phases. The second stage of the thermal treatment is a slow solidification process which consists in melting again the ingot in the same crucible, under argon atmosphere, near above the solidus temperature (1273 K) and then in slowly pulling the crucible out of the heating zone of the induction coil (Bridgman-type technique) at a rate of 2–6 mm/h. The final ingot contains an important distribution in sizes of decagonal needles which have grown inside cavities. Arguments for the growth mechanism are based on the knowledge of icosahedral short-range order in overheated liquids and of a large quantity of vacancies in aluminium-rich alloys: they will be published elsewhere.[15]

Single-crystal x-ray diffraction patterns were carried

 

out on $Al_{63}Cu_{17.5}Co_{17.5}Si_2$ decaprisms (volume: $10^{-3}$–$10^{-4}$ $mm^3$), performing rotating crystal or precession experiments, with conventional x-ray sources (Mo or Cu anodes) and with synchrotron radiation at LURE (Orsay, France). The crucial role of high-resolution x-ray diffraction patterns (experiments using synchrotron radiation) will be emphasized in the paper.

### B. Experimental results

A rotating crystal experiment was made with the needle axis parallel to the imaging film, using Mo $K\alpha$ radiation: $\lambda = 0.711$ Å. The diffraction pattern (Fig. 1) exhibits layers of Bragg spots. After standard geometrical correction, they are found equidistant: samples are periodic along their longitudinal axis, with a periodicity $c = 4.13$ Å. Between the layers of Bragg spots there are layers of diffuse scattering, corresponding to twice the period.

The tenfold symmetry of the layers was displayed using the precession technique for which a reciprocal plane is selected and restored on the imaging film without any deformation. The $l = 0$, $l = \frac{1}{2}$, and $l = 1$ reciprocal planes perpendicular to the **c*** direction are shown on the diffraction patterns in Fig. 2, the x-ray wavelength was equal to 0.711 Å. In this paper only Bragg peaks will be taken into account in the data analysis but, nevertheless, you will note the peculiar structure of the $l = \frac{1}{2}$ diffuse scattering plane, which exhibits "Christmas trees" similar to those observed for decagonal $Al_{70}Ni_{15}Co_{15}$.[16] Enlarged small-$Q$ areas of the $l = 0$ plane are obtained (i) using conventional x-ray source, for Cu $K\alpha$ radiation ($\lambda = 1.542$ Å) (Fig. 3), (ii) using synchrotron radiation ($\lambda = 1.495$ Å) (Fig. 4): "high-resolution" experiments.

Although Al-Cu-Co(-Si) SK samples[14] and our samples[9,10] have slightly different nominal compositions [(65/20/15/0) for (63/17.5/17.5/2)], their $l = 0$ and $l = 1$ reciprocal planes (obtained for Mo $K\alpha$ radiation) are very similar (SK data are known from the list of structure factors, available upon request).[14(a)] This similarity is evidenced by comparing, for example, Fig. 2(a) in this paper and Fig. 1(a) in Ref. 14(a). Nevertheless, SK data were interpreted within the scope of a quasicrystalline model[14] whereas our data were interpreted within the scope of a microcrystalline model.[9,10] Consequently, in Secs. III and IV, we present a detailed analysis of our data within

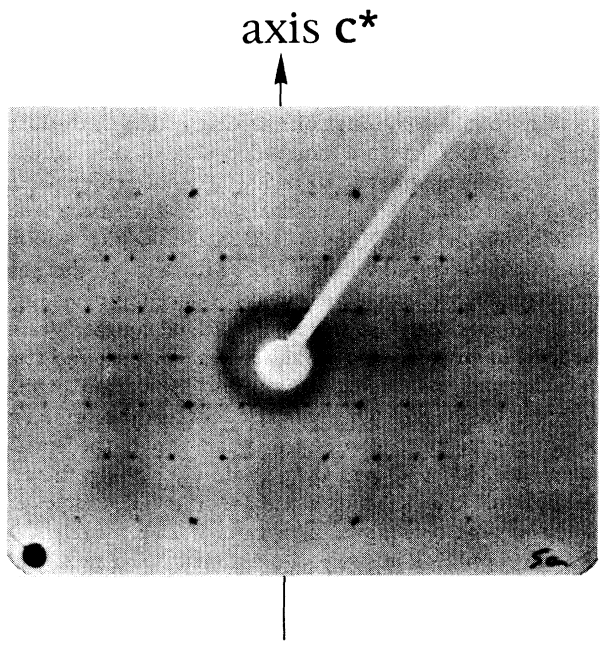


FIG. 1. Monochromatic rotating crystal pattern of decagonal $Al_{63}Cu_{17.5}Co_{17.5}Si_2$: $\lambda = 0.711$ Å (Mo $K\alpha$ radiation), the wavelength is selected using the (0,0,2) reflection of a pyrolytic graphite monochromator, $\lambda/n$ ($n = 2,3$) contaminations are avoided by choosing adequate generator voltage. The needle axis is parallel to the pattern.

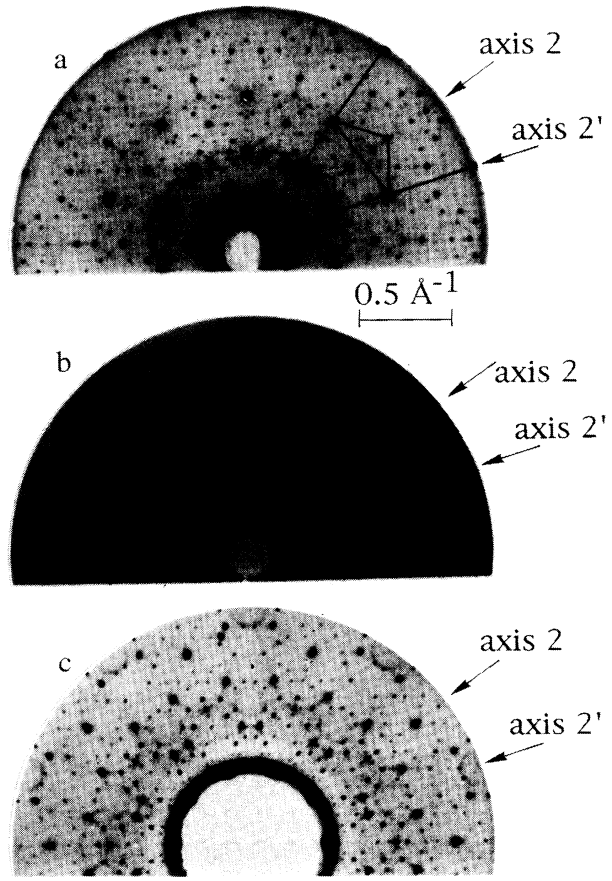


FIG. 2. Monochromatic x-ray precession patterns of decagonal $Al_{63}Cu_{17.5}Co_{17.5}Si_2$ obtained using Mo $K\alpha$ radiation ($\lambda = 0.711$ Å), the wavelength is selected using the (0,0,2) reflection of a pyrolytic graphite monochromator, $\lambda/n$ ($n = 2,3$) contaminations are avoided by choosing adequate generator voltage. (a) $l = 0$ reciprocal plane (zero level reciprocal plane perpendicular to the periodic axis **c***). The sample-film distance is 60 mm. We refer to solid and dotted line pentagons in Sec. V. (b) $l = \frac{1}{2}$ reciprocal plane: diffuse scattering. (c) $l = 1$ reciprocal plane: note the pseudoextinction observed along one of the two types of twofold axes (termed 2'). Scales are indicated in the picture: in this paper, all reciprocal vectors are defined without $2\pi$ factor.

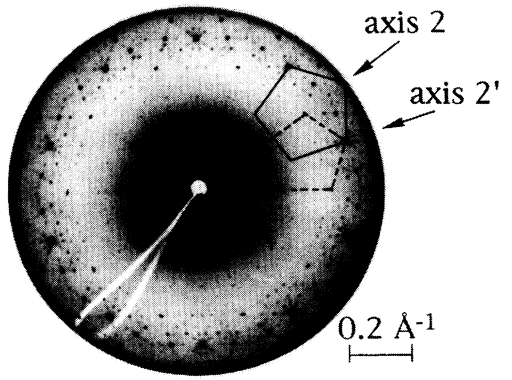


FIG. 3. Monochromatic x-ray precession pattern obtained from the $l=0$ reciprocal plane perpendicular to the periodic axis $\mathbf{c}^*$ using Cu $K\alpha$ radiation [$\lambda=1.542$ Å, the wavelength is selected using the (0,0,2) reflection of a pyrolytic graphite monochromator, some very weak reflections may be due to small contaminations by $\lambda/2$ or $\lambda/3$ radiations; the sample-film distance is 60 mm].

the scope of the two models in order to discriminate between the two possible interpretations.

## III. DATA ANALYSIS WITHIN THE FRAMEWORK OF A QUASICRYSTALLINE STRUCTURAL MODEL

After a brief summary of quasicrytalline models in Sec. III A we will concentrate on the model of SK.[14] In Sec. III B, the main features of their hyperspace description will be summed up and the resulting direct space atomic decoration will then be discussed. In Sec. III C, the intensity cutoff problem, for quasicrystal structure determination, will be pointed out from the example of their model. In Sec. III D, we shall attempt to analyze our x-ray diffraction data within the same framework.

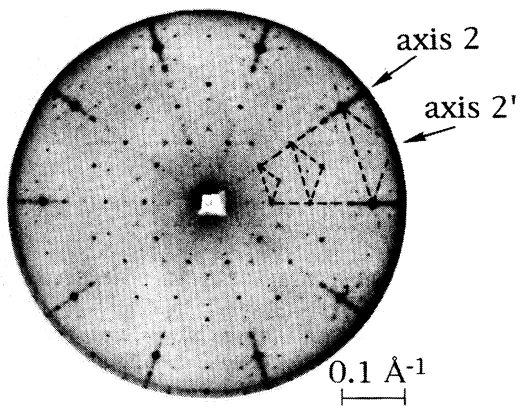


FIG. 4. Monochromatic x-ray precession pattern obtained from the $l=0$ reciprocal plane perpendicular to the periodic axis $\mathbf{c}^*$. The x-ray wavelength $\lambda=1.495$ Å is selected using the (1,1,1) reflection of a germanium monochromator (no $\lambda/2$ contamination). The sample-film distance is 125 mm and beam collimation is better than for experiments with standard x-ray sources. This pattern obtained with synchrotron radiation is a better resolution one. Spots 1 have the strongest intensity.

### A. Al-Cu-Co(-Si) quasicrystalline structural models

Quasicrystals are usually described either on the basis of deterministic models (within the framework of the cut-and-projection method[3,17–19] or with decorated quasiperiodic tilings[20,21]) or on the basis of random tiling models.[22–24] We will not discuss random tiling models in the present paper.

Let us mention three deterministic models which were developed to describe decagonal Al-Cu-Co(-Si): the Steurer-Kuo model,[14] the Burkov models,[25] and the Daulton-Kelton model.[26] They are discussed in Ref. 21 which presents current models of decagonal atomic structures.

The structural model of Steurer and Kuo[14] is derived from the Penrose tiling: it is formulated within the same cut-and-projection formalism. It was derived from the analysis of single-crystal x-ray diffraction data. It is thus of special interest for us, because it is based on results which can be directly compared to our results. In this paper it is this model which is nearly exclusively discussed and which is used for our experimental data analysis.

Burkov models are deduced from more theoretical considerations, the starting point being the existence of "decagonal" clusters. They are formulated in a decorated tiling formalism or in hyperspace formalism. It might be interesting in the future to apply such a description to the analysis of our experimental data.

The Daulton and Kelton model gives an atomic description of the relationships existing between the decagonal phases with different $c$ periodicities[4] by fitting together distorted icosahedra but it does not describe how quasiperiodic order spreads out at large distances in the decagonal planes and cannot be applied to discuss the results of our experiments.

### B. Hyperspace and real-space descriptions of the Steurer-Kuo model

The two-dimensional (2D) Penrose tiling is a quasiperiodic packing of two kinds of rhombs: a large one, with an acute 72° angle and a small one, with an acute 36° angle. It can be built using matching rules, a deflation procedure, or the cut-and-projection method. Only this last method will be used in this paper. We will summarize the main features necessary for the understanding of the SK model, the detailed calculations being developed in Refs. 18 and 27–30, and references therein.

The Penrose rhomb vertices can be determined by cutting a 5D hypercubic lattice[31] the edge length of which is noted $d_s$. In the 3D perpendicular space, the "atomic" volume is a rhombic icosahedron, which is connected to the hyperlattice points by a vector $\mathbf{Y}$. As proved by Jaric in Ref. 27, tilings satisfying the relation $\sum y_i=0$, where $y_i$ ($i=1-5$) are the coordinates of $\mathbf{Y}$, have the same diffraction patterns. Consequently, when respecting the condition $\sum y_i=0$, the knowledge of the diffraction patterns does not give any information about the "origin" $\mathbf{Y}$. For most quasicrystals in the present work, atomic volume is placed at the point $\mathbf{Y}_0$ defined by $y_1=\frac{1}{3}$,

$y_2=-\frac{1}{7}, y_3=\frac{1}{11}, y_4=-\frac{1}{13}, y_5=-\sum_{y_k}$ $(k=1-4)$. It corresponds to a generic origin and it does not lead to singular Penrose lattices.

Hyperlattice points do not project densely onto the fivefold axis of the rhombic icosahedron but only fall onto equidistant points; on the contrary, orthogonal sections of the rhombic icosahedron through these points are densely filled. So, only these sections are in fact used as atomic surfaces. For **Y** satisfying the condition $\sum y_i=0$ $(i=1-5)$, one gets four pentagonal equidistant sections as shown, for instance, in Fig. 7 in Ref. 27; surfaces of the four pentagons are respectively equal to $d_s^2\sin(72°)$ for the first and the fourth ones and to $\tau^2 d_s^2\sin(72°)$ for the second and the third ones, $\tau$ being the "golden mean" $[\tau=2\cos(36°)]$. Correlatively, in 2D parallel space, projected basis vectors point towards the vertices of a regular pentagon and their sum is equal to zero: one among the five dimensions is redundant. One can restrict the 5D cubic hyperspace to a 4D oblique one via a section perpendicular to the fivefold axis of the rhombic icosahedron. One gets the above-mentioned four pentagons. They are located at the four Wyckoff positions: $(\nu/5)(1,1,1,1)$, $\nu=1,2,3,4$, in the basis of the 4D oblique lattice. See Fig. 5(a). Intersection points of the pentagons with the parallel space are the vertices of the Penrose tiling [Fig. 5(b)]. Edge lengths of the rhombs are equal to $(\sqrt{2}/\sqrt{5})d_s$.

Using the hyperspace formalism of the Penrose tiling and single-crystal diffraction data, SK proposed a structure for the quasicrystalline $Al_{65}Cu_{20}Co_{15}$. For details

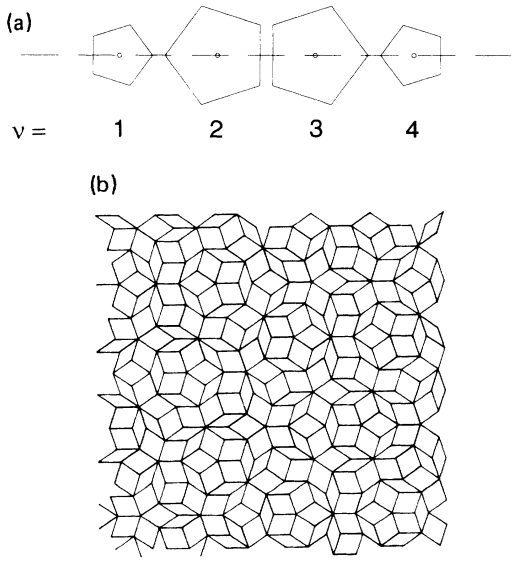


FIG. 5. Penrose tiling. (a) Schematic representation of the four pentagonal surfaces in perpendicular space [Wyckoff positions $\nu/5(1,1,1,1)$, $\nu=1,\ldots,4$]. Relative sizes and orientations of the pentagons are respected but not their relative positions. For a better understanding of their positions, see, e.g., Fig. 7 in Ref. 27, where the rhombic icosahedron and its pentagonal sections are drawn. (b) Penrose tiling with 36° and 72° rhombs, the vertices are the intersection points of the perpendicular space surfaces with parallel space.

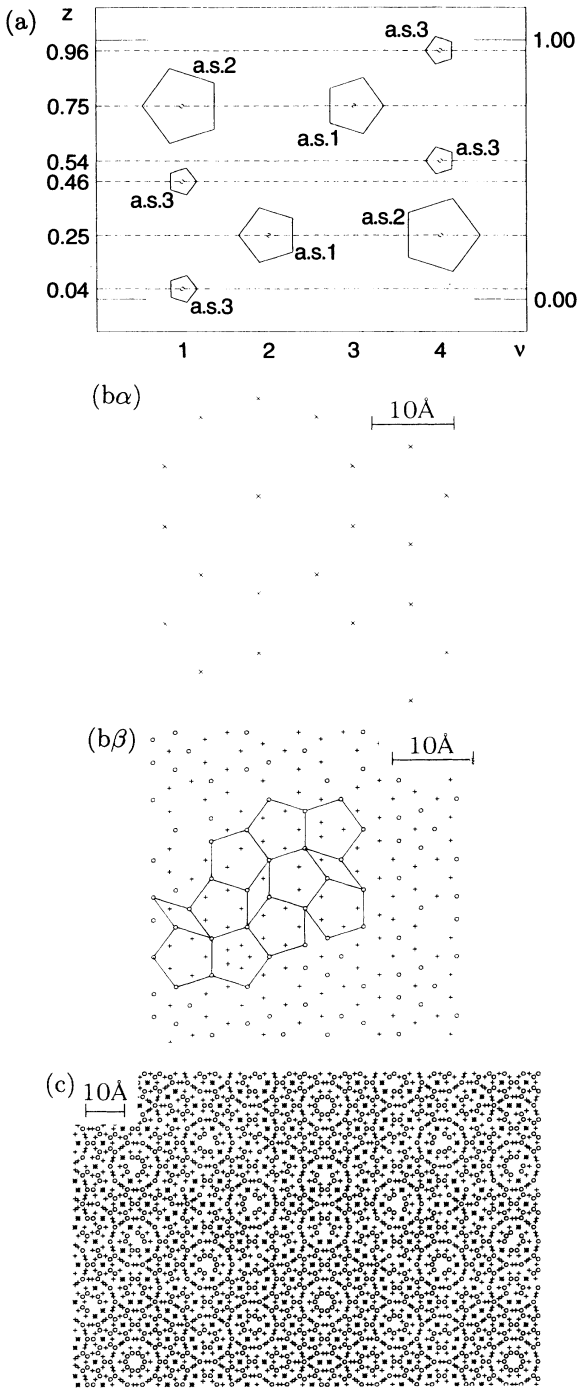


FIG. 6. Decagonal $Al_{65}Cu_{20}Co_{15}$: SK model. (a) Schematic representation of the hyperunit cell of the SK model [Ref. 14(a)] [eight atomic surfaces ("a.s."), three of which are independent]. (b) Atomic planes in parallel space: $(\alpha)$ the plane at $z=0.04$ coordinate in the $c$ direction, the atomic sites of which are selected by "a.s. 3", $(\beta)$ the $z=0.25$ plane, the atomic sites of which are selected by "a.s. 1" and "a.s. 2". Solid lines point out the similitude with Fig. 7(a) in Ref. 14(a). (c) Projection along the $c$ axis of the atomic planes. All atomic positions are represented without taking into account their occupancy factors. Circle, "a.s. 1" (Cu/Co:92%, Al:8%); horizontal cross, "a.s. 2" (Al only, occupancy factor: 86%), turned cross, "a.s. 3" (Al only, occupancy factor: 25%). These drawings are made for the origin $\mathbf{Y}_0$ (see the definition of this origin in Sec. III B).

about the structure refinement method used (Patterson and Fourier syntheses), the reader is referred to Ref. 14 and to the review papers.[3,19]

The used hyperspace is the 4D Penrose hyperspace plus the periodic direction c: perpendicular space is 2D and physical space (parallel space) is 2D plus the periodic direction. The hyperspace group was found to be $P10_5/mmc$ with an hyperscrew axis along the periodic direction $c$, the hyperscrew axis and $c$-glide planes were deduced from systematic extinction of peaks $(h_1,h_2,-h_2,-h_1,l)$ for $l=2n+1$ (Ref. 14) [cf. axes 2′ in Fig. 2(c)]. The parameters of the hyperunit cell are $d_s=2.381$ Å and $c=4.148$ Å. The Patterson analysis led to the determination of the positions of three independent pentagonal atomic surfaces located at the Wyckoff positions: $(\nu/5)(1,1,1,1,0)+(0,0,0,0,z)$, where the $z$ coordinate corresponds to the periodic direction c. For "atomic surface 1," $\nu=2$ and $z=0.25$, for "atomic surface 2," $\nu=4$ and $z=0.25$, for "atomic surface 3," $\nu=1$ and $z=0.04$; there are six atomic planes within the period $c$ in parallel space. Subsequent least-squares refinement has led to refined values concerning the atomic surfaces which are given in Table I of Ref. 14(a).[32] For atomic surface "$k$" ($k=1,2,3$), SK determined the radial atomic size $\lambda_k\times 3.765$ Å, the total site occupancy $p_k$ and the partial Al-occupancy factor $p_k$(Al): $\lambda_1=-0.335$, $p_1=1$, $p_1$(Al)$=0.08$, $\lambda_2=0.444$, $p_2=0.86$, $p_2$(Al)$=1$, $\lambda_3=0.16$, $p_3=0.25$, $p_3$(Al)$=1$ (negative $\lambda_k$ denotes opposite pentagon orientation).

A schematic representation of the hyperunit cell and portions of the atomic planes $z=0.04$ and 0.25 in parallel space are shown in Figs. 6(a) and 6(b). The contents of the $z=0.04$ and 0.46 planes are the same and the $z=0.54$ and 0.96 planes are related to the previous ones by the hyperscrew and mirror operations. The $z=0.25$ and 0.75 planes are also related one to the other by these symmetry elements. So the projection of all the atoms on a single plane gives rise to pseudodecagonal atomic rings [see Fig. 6(c)].

Let us now discuss the atomic structure in direct space when calculated by cutting the hyperspace structure. The existence of (pseudo-)decagonal rings shown in Fig. 6(c) is an important point, which was first pointed out by Burkov:[25(a)] high-resolution electron microscopy micrographs also show decagonal rings in projection along the c axis (see, e.g., Refs. 11 and 33). Nevertheless, note that in Fig. 6(c) decagonal ring symmetry is often uncompleted, which is not the case in Burkov models.[25]

The SK model leads to a density $\rho=4.4$ g/cm$^3$,[14] in rather good agreement with measured density[34] $\rho\approx 4.7$ g/cm$^3$. Some discrepancies appear when precise atomic environments are studied. Indeed, (i) extended x-ray absorption fine-structure study of quasicrystalline $Al_{65}Cu_{20}Co_{15}$ (Ref. 35) shows that the near-neighbor structures around Co and Cu consist of $9\pm 2$ Al atoms at distances of $2.43\pm 0.03$ and $2.47\pm 0.03$ Å, respectively; (ii) from the SK model, we calculate that the distance between a Cu/Co atom and its nearest Al neighbors is effectively 2.44 Å but that only a small number of Al atoms are concerned, the next Al neighbors being located at a distance of 2.56 Å.

Moreover, nonphysically short Al-Al bonds of 1.2 or 1.77 Å are calculated (see, e.g., pair potentials of Refs. 36 and 37 and references therein). These results are obtained without any correlations between atomic occupancy factors of surfaces "2" and "3" for instance. As suggested by SK Fourier analysis [Fig. 7 in Ref. 14(a)], such correlations may exist and, if taken into account, they would probably allow one to improve the model from the point of view of chemical bonding.

Direct space structure deduced from the SK model can also be discussed with regard to channeling experiments.[38–40] Comparison of experimental ion channeling profiles with those calculated on the basis of the SK model indicate that Co and Cu do not play the same role, which should be incorporated in the quasicrystalline model.[39] Electron channeling experiments also show that some Al atoms may be found slightly out of the $z=0.25$ and 0.75 planes,[40] which may be related to the large Debye-Waller factor relative to the c direction found by SK for "atom 2" (indeed, Debye-Waller factors may account not only for phonon-type fluctuations but also for static disorder).

Despite of the above discrepancies, the SK model remains, at the present time, one of the most advanced models developed to understand the structure of quasicrystalline Al-Cu-Co and we will use it to analyze our diffraction data in Sec. III D.

### C. The intensity cutoff problem in quasicrystal structure determinations

In structure refinements, a reliability factor is defined:

$$R=\sum\|F_{\rm obs}|-|F_{\rm calc}\|\Big/\left\{\sum|F_{\rm obs}|\right\},$$

where $F_{\rm obs}$ is the measured structure factor of a diffraction peak, $F_{\rm calc}$ the calculated one; the sum runs over all observed independent peaks, the number of which is as large as possible. The smaller the reliability factor is, the better the structure refinement.

Let us underline a general problem regarding structure refinements of quasicrystals on the example of the SK model.[14(a)] In quasicrystals the reciprocal space contains a dense set of diffraction peaks. There may happen that, after refinement of the quasicrystal structure, the calculation of the reciprocal space, starting from the refined structure model, generates diffraction peaks the intensities of which are higher than the smallest peak intensity measured in the experiment although they have not been looked for during the experiment. Indeed, when calculating[41] for instance the $l=0$ diffraction pattern corresponding to the SK model with their experimental cutoff in intensity, we find that the model predicts numerous peaks the intensities of which are higher than the sensibility threshold of the experiment but which have not been measured (see Fig. 7). These peaks are not taken into account in the structure refinement where the reliability factor is calculated as a sum over the observed peaks and information is then lost. It means that the classical experimental method, which consists of measuring a data set and the subsequent refinement of the structure from this data set, must be reconsidered for quasicrystals.

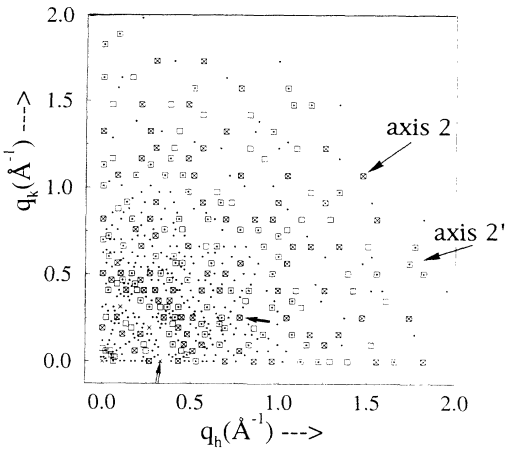


FIG. 7. $l=0$ diffraction plane of quasicrystalline $Al_{65}Cu_{20}Co_{15}$. The squares represent the peaks measured by SK [Ref. 14(a)] (cf. the list of experimental data disponible upon request). $I_0$ being the intensity of the strongest peak measured in the $l=0$ plane (see the peak indicated by an arrow), we have reported calculated peaks for the intensity ratio $I/I_0 \geq 0.0008$ [experimental cutoff in Ref. 14(a)]. They are represented by crosses for $I/I_0 \geq 0.01$ and by dots for $0.0008 \leq I/I_0 < 0.01$. This figure shows that many calculated peaks have not been measured, even, for example, the relatively strong one indicated by a double arrow. On the contrary, some measured peaks, while corresponding to well-defined quasicrystalline positions, would require a smaller cutoff value to be interpreted.

Indeed, it should, namely, include further stages: (i) the calculation of the diffraction patterns within the experimental intensity cutoff, (ii) additional measurements at the calculated peak positions for the peaks not found in the previous measurements, (iii) additional refinements taking into account these peaks (whether it be observed or not). This procedure should be iterated until convergence.

### D. Failure of the quasicrystalline model concerning the analysis of our experimental results

Our diffraction data obtained with conventional x-ray sources [Figs. 2(a), 2(c), and 3] present similarities with SK data (comparison was made in a quantitive way for peak positions but only in a qualitative way for peak intensities because all peak intensities in our imaging films were not studied quantitatively). Moreover, we have shown previously that the indexation of peak positions in Figs. 2(a) and 3 was possible within the scope of a microcrystalline model.[9] So in order to discriminate unambiguously between a quasicrystalline or a microcrystalline state, we performed a "high-resolution" x-ray diffraction experiment: see Fig. 4 and Ref. 10.

Figure 8 displays the diffraction peak positions generated within the scope of the SK model[14(a)] for an intensity cutoff equal to $5\times10^{-4}$ (our experimental cutoff, without taking into account either Lorentz or absorption corrections) and for a much smaller cutoff equal to $10^{-4}$. Peak positions measured on the high-resolution x-ray diffraction pattern are reported in the same figure. Many experimental peaks are not fitted, which evidences some discrepancy between the model predictions and our experimental results. So let us also consider the problem from a complementary approach. A reciprocal plane of a quasicrystal is a dense set of peaks: taking into account experimental precision in peak position determination, each peak in the plane can be indexed. Nevertheless detectable peaks are locally isolated in a background of nondetectable peaks of too weak intensities (see, e.g., calculated peaks in Fig. 7): the detectable peaks must be indexed by a combination of sufficiently small indices in the hyperspace basis. Figure 9 plots the percentage of fitted peak positions for the peaks of the high-resolution diffraction pattern versus the SK reciprocal basis vector length $a^*$. If reciprocal space positions are generated for hyperspace indices varying between $-10$ and $+10$, only 30% of the experimental peak positions are fitted and for indices varying between $-30$ and $+30$, 10% of them are still not fitted. Although Fig. 4 is relative to a smaller wave-vector area than SK data, noting that all peak positions measured by these authors are fitted for indices

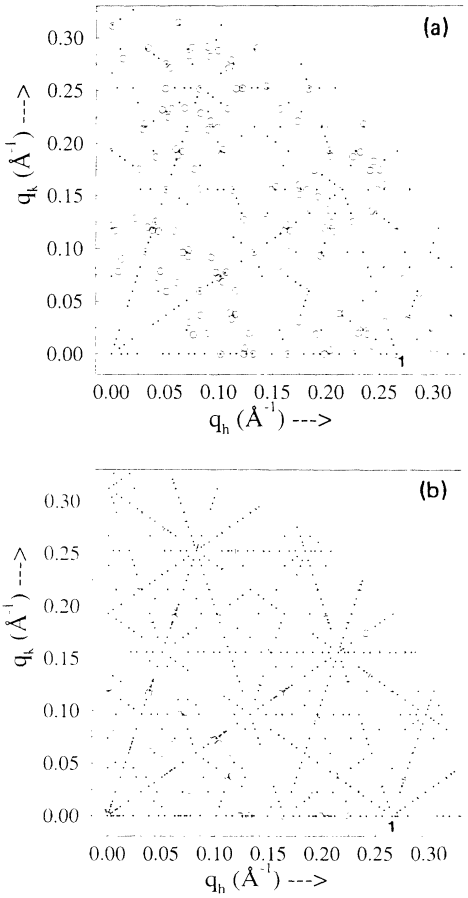


FIG. 8. $l=0$ diffraction plane in the area of small wave vectors. The circles represent peak positions measured from the high-resolution x-ray diffraction pattern shown in Fig. 4 (peaks resulting from $\lambda/3$ and $\lambda/4$ contaminations have been suppressed). The dots represent peak positions calculated from SK model [Ref. 14(a)]. (a) For our experimental cutoff $I/I_0 \approx 0.0005$, $I_0$ being the intensity of the strongest peak, peak "1" in Fig. 4 (peak intensities are obtained by taking photographs of various duration in order to avoid saturation effects). (b) For an even smaller cutoff: $I/I_0 = 0.0001$.

varying between $-3$ and 3,[14] one concludes that the sets of indices in Fig. 9 are really large. This observation clearly demonstrates that our data cannot be interpreted within the scope of the SK model.

## IV. DATA ANALYSIS WITHIN THE FRAMEWORK OF A MICROCRYSTALLINE MODEL

In the first subsection, we will set out the microcrystalline model. In the second subsection, we will present the analysis of our data within the scope of this model.

### A. The microcrystalline model

Just after the discovery of quasicrystals, their true existence was debated (see, e.g., Ref. 42). Indeed, apparent icosahedral or decagonal symmetries can also be due to multiple twinning.[42–47]

It is one of the components of the microcrystalline model: we consider crystalline domains with well-defined orientational relationships which restore forbidden crystallographic symmetry in reciprocal space. For instance, in the decagonal case, they restore a perfect tenfold symmetry.[45–47] In particular, a decagonal microcrystal can be constructed from domains the unit cell of which is a 72° rhomb in the plane perpendicular to the $c$ axis [Fig. 10(a), Ref. 46]: the domains are rotated relative to each other by 72° in direct space and peak positions in reciprocal space are calculated by superimposing the reciprocal lattices of the five rotated domains [Fig. 10(b)].

Another important component of the microcrystalline model is the domain unit-cell decoration.[47] Indeed, microcrystals have been discovered in alloys which are quasicrystals for a slightly different composition or a different temperature range and local atomic order was found to be very similar between the microcrystal and the quasicrystal, this has been shown for example from x-ray diffraction data.[9,48,49] Very similar atomic order between a domain unit cell and the quasicrystal means that each domain in the microcrystal is an approximant of the quasicrystal (for a review paper on approximants, see, e.g., Ref. 50).

The third component of the microcrystalline model concerns the domain coherence. Although the microcrystal is formed of crystalline domains, difficult problems are raised when one tries to take into account the arrangement of the domains with possible coherence between them. They will be discussed in Sec. V. In brief, a microcrystal is formed of twins of crystalline coherent domains of approximant phase.

Characteristics of a microcrystal diffraction pattern are illustrated in Fig. 11. A single-domain approximant of the Penrose tiling is drawn in Fig. 11(a). Its calculated diffraction pattern is reported in Fig. 11(b). Strong peaks have nearly the same position and intensity as those of the quasicrystalline Penrose tiling [compare with Fig. 11(c)], but some weak peaks clearly show deviations from the perfect tenfold symmetry. On the other hand, diffraction patterns of a microcrystal, which consist of

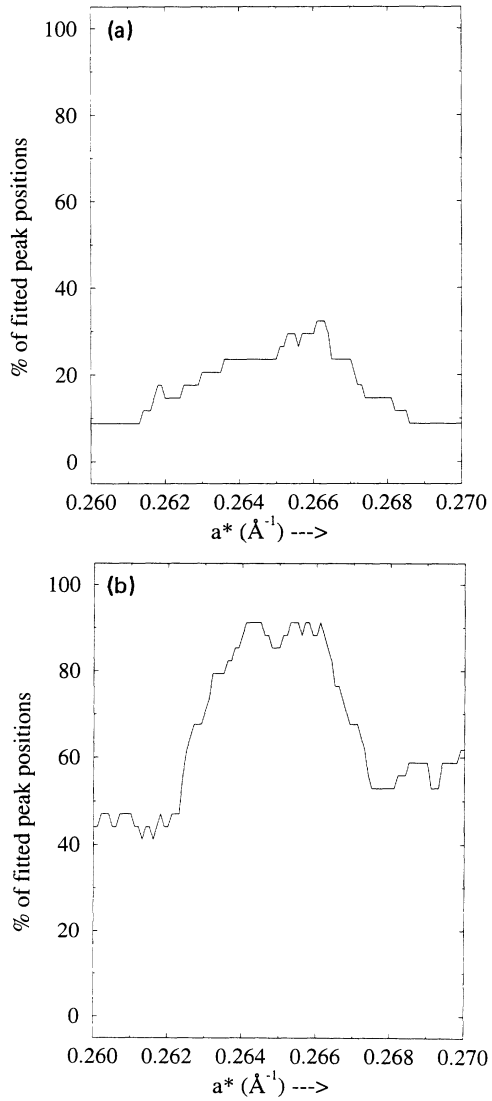


FIG. 9. Percentage of fitted peak positions of Fig. 4 as a function of the reciprocal length $a^*$ of the SK basis ($a^*=0.2656$ Å$^{-1}$ in Ref. 14): (a) for quasicrystalline peaks generated for hyperspace indices varying between $-10$ and $+10$, (b) for quasicrystalline peaks generated for hyperspace indices varying between $-30$ and $+30$. Peak positions are measured with a precision of 0.002 Å$^{-1}$.

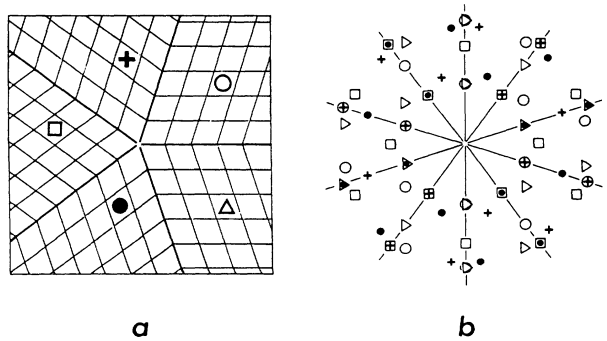


FIG. 10. Microcrystalline example: (a) orientational relationships between domains formed of 72° rhombs; (b) corresponding diffraction peaks: peak positions are calculated by superimposing the reciprocal lattices of the rotated domains.

adequately twinned approximant domains, exhibit perfect tenfold symmetry [see Fig. 11(d)]. Hence, the characterization of quasicrystalline and microcrystalline states can be an experimental challenge, as will be illustrated in Sec. IV B. With regard to diffraction patterns, we must lay emphasis on the existence of multiple components in microcrystal strong diffraction peaks. Indeed, strong diffraction peaks of a single domain of the approximant type being very close to those of the quasicrystal, the superimposition of the diffraction patterns of, e.g., five types of domains turned relative to each other by 72° leads to sets of five very close peaks [see Fig. 11(d)]: strongest peaks of microcrystal diffraction patterns are multicomponent peaks.

### B. Data analysis

Some of the results have already been published in Refs. 9 and 10 but the present analysis is more extensive and gives a better understanding of the structure and of related questions. In a first stage,[9] we analyzed the data of Figs. 2(a) and 3 ($l=0$ diffraction plane, conventional x-ray sources). Two microcrystalline models were chosen to try to fit the diffraction peak positions: (i) domains tiled with a rhomb of edgelength $r$ and acute angle 36°, orientational relationships between domains consisting in 36° rotations [Fig. 4(a) in Ref. 9], (ii) domains tiled with a rhomb of edgelength $r$ and acute angle 72°, orientational relationships between domains consisting in 72° rotations [Fig. 10(a)]. The peak positions are calculated by superimposing the rotated reciprocal lattices of the domains. Four different unit cells have allowed the fitting of all the data: 36° rhombs with edges $r_0$ and $r_0/\tau$ ($r_0=51.5$ Å) and 72° rhombs with edges $r_0$ and $r_0/\tau$ [see Fig. 5 in Ref. 9]. As previously underlined,[9,48] similitudes between our diffraction patterns and quasicrystalline diffraction patterns show that these unit cells must be of the approximant type. At the time of these first experiments, resolution was not good enough to distinguish unambiguously between a microcrystal and a quasicrystal and in the case of a microcrystal between the four unit cells.[9,52,53]

To get conclusive results, "high-resolution" x-ray

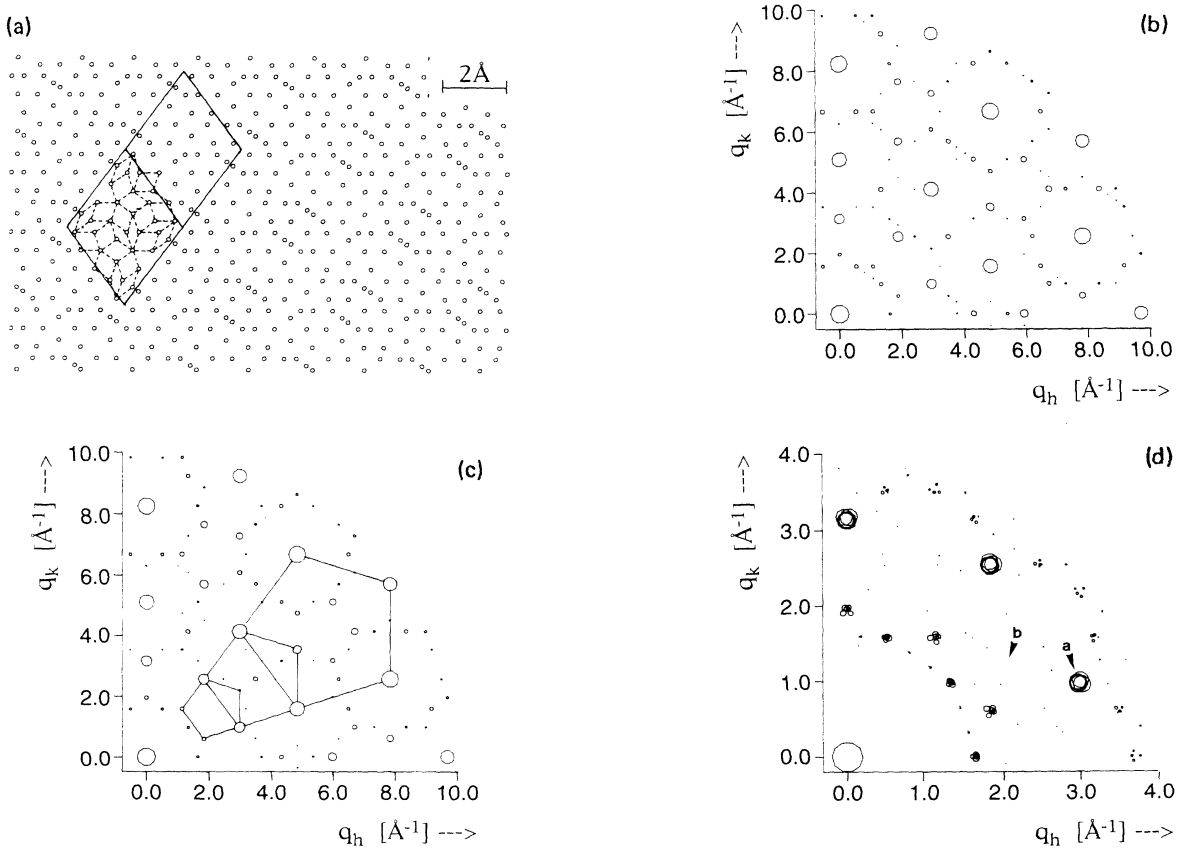


FIG. 11. (a) (1,3) Penrose approximant [notation (1,3) from Ref. 51]. Its rhomb unit cell is indicated by solid lines: its edge is equal to 3.1495 Å; edges of small rhombs inside are equal to $\sqrt{2}/\sqrt{5}$ Å ($d_S=1$ Å). This drawing is made for the origin $Y_0$ (see the definition of this origin in Sec. III B). (b) Its diffraction pattern for an intensity cutoff $I/I(Q=0)$ equal to $10^{-2}$. Atomic scattering factors are equal to one for each vertex. Spot radii are proportional to peak intensities. (c) Diffraction pattern of a quasicrystalline Penrose tiling with rhomb edge equal to $\sqrt{2}/\sqrt{5}$ Å ($d_S=1$ Å). Atomic scattering factors are equal to 1 for each vertex. The cutoff $I/I(Q=0)$ is chosen equal to $10^{-2}$. Spot radii are proportional to peak intensities. (d) Superimposition of the diffraction patterns [from (b)] of five approximant domains rotated relative to each other by 72°. Strong rotated peaks are very close to each other (see, e.g., peak "*a*") and are difficult to resolve in a diffraction experiment. Other peaks (e.g., peak *b*) are single-component peaks.

diffraction experiments[10] were performed. Resulting $l=0$ precession pattern is shown in Fig. 4. Comparison between the different possible microcrystalline unit cells can be inferred from Fig. 12, which gives the percentage of fitted peak positions for 36° and 72° rhombs: only the microcrystal constructed from five rotated domains formed of rhombs with acute angle 72° and with edge $r_0=51.515$ Å fits the whole set of experimental peak positions. Comparison between measured and calculated peak positions is shown in Fig. 13. Although this result does not eliminate the possibility of the coexistence of domains tiled with an $(r_0,36°)$ rhomb, for example, it makes it unlikely. In agreement with an $(r_0,72°)$ microcrystal, note also that peak positions in the $l=1$ plane, deduced from Fig. 2(c), are all fitted within the scope of this microcrystalline model.

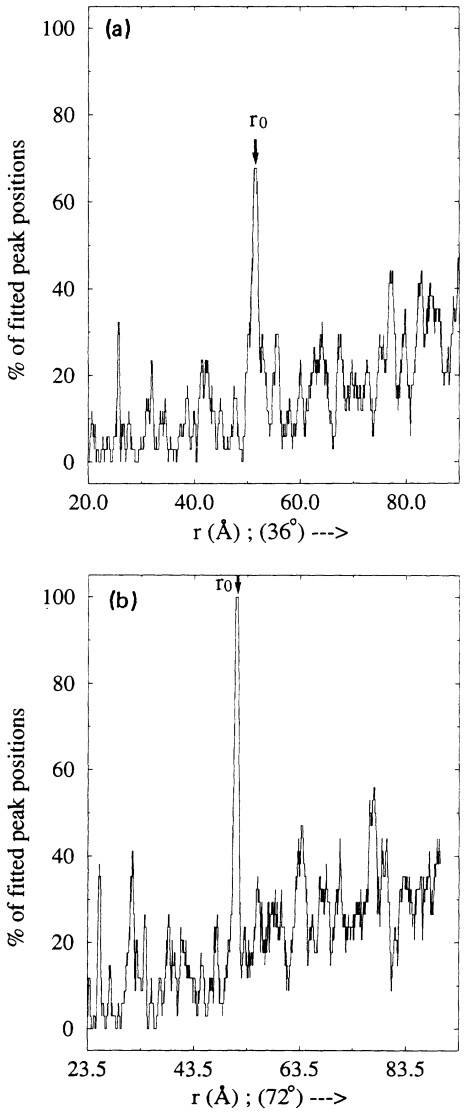


FIG. 12. Percentage of fitted peak positions of Fig. 4 as a function of the edge-length $r$ of the rhomb unit cell within the framework of the microcrystalline model: (a) with a 36° angle, (b) with a 72° angle. Peak positions are measured with a precision of 0.002 $Å^{-1}$. All peak positions are fitted in (b) for $r_0=51.515$ Å.

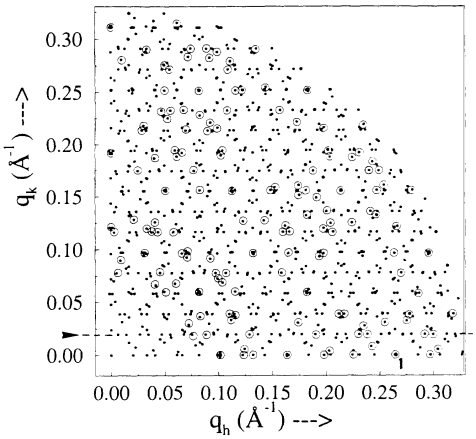


FIG. 13. Comparison between measured and calculated peak positions (circles and dots) for the nondecorated microcrystal formed of domains with ($r_0=51.515$ Å, 72°) rhombs, the domains being rotated relative to each other by 72°. Peaks resulting from $\lambda/3$ and $\lambda/4$ contaminations have been suppressed. Note the dotted line constructed from measured diffraction peaks: it corresponds to the $(0,\pm1,0)$ reciprocal planes coming from two of the five types of crystalline domains (the rhomb unit-cell parameters being $a=b=51.515$ Å, $\gamma=108°$).

So, our experimental data show that our sample is in a microcrystalline state, the domain unit-cell parameters being $a=b=51.515$ Å, $c=4.13$ Å, and $\gamma=108°$ [which corresponds to the (51.515 Å,72°) rhomb in the plane perpendicular to the $c$ axis].[54–57] Please note that the same microcrystalline state was found in Al-Cu-Co alloys using transmission electron microscopy techniques.[8]

Such periodic 2D structure can be easily related to the approximants of 2D Penrose-type lattices as studied in Refs. 51 and 58. Following the method developed by Edagawa, Suzuki, Ichihara, and Takeuchi[51] which consists of changing the slope of the selection window, one finds for the $(k,k')$ approximant the following parameters: $a=d_s(\sqrt{2}/\sqrt{5})(2\tau-1)\tau^{k+1}$ and $b=d_s(\sqrt{2}/\sqrt{5})\sqrt{(3-\tau)}\tau^{k'+1}$, where $a$ is normal to $b$; $d_s$ is the hyperunit-cell parameter ($d_s=2.381$ Å). If $k$ and $(k'+1)$ are equal modulo 3, the unit cell is centered and the primitive unit cell is a rhomb. The $(r_0=51.5$ Å,72°) rhomb in microcrystalline Al-Cu-Co-Si is then found to correspond to a (5,7) approximant. Three-dimensional $(k,k')$ approximants for which the $c$ direction is taken into account can also be constructed with the help of the Edagawa *et al.* method, starting from a hyperspace description in which the periodicity $c$ is included.

It is important to test the effect of the unit-cell decoration on Fig. 13 results. Indeed, Fig. 13 shows that measured peak positions are fitted within the scope of the nondecorated microcrystalline model, but that numerous calculated peaks were not observed in the experiment. To introduce the unit-cell decoration, we started from the SK quasicrystalline model: a (5,7) approximant is calculated in Fig. 14(a). The rhomb unit-cell decoration is, indeed, very similar to the decoration found in some part

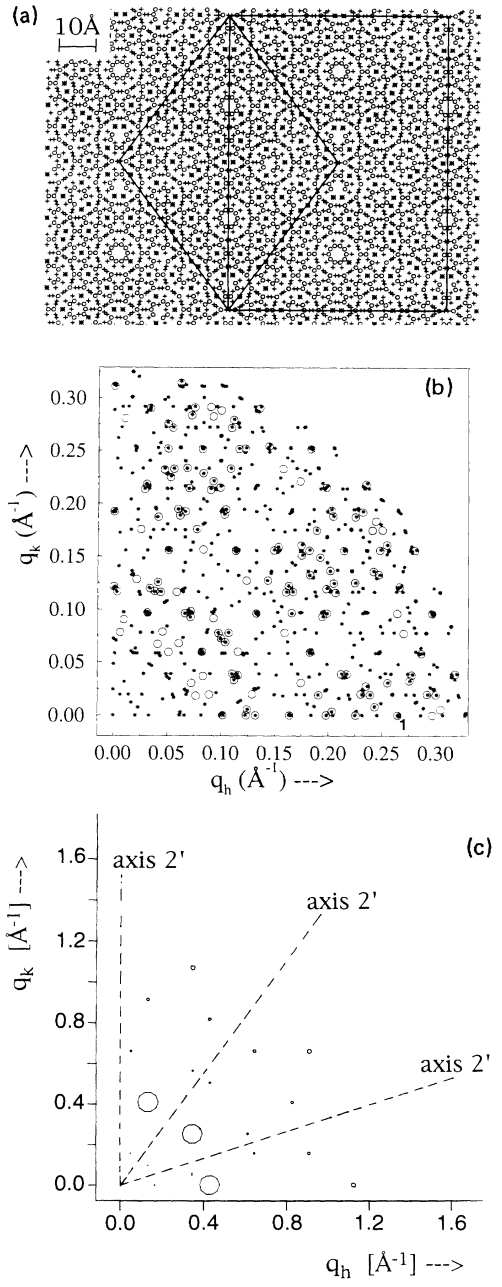


FIG. 14. (a) Part of a single domain of a (5,7) approximant of the SK model [Ref. 14(a)] in projection along the $c$ axis (origin $\mathbf{Y}_0$; see the definition of this origin in Sec. III B). All atomic positions are represented without taking into account their occupancy factors. Circle, atomic sites selected by "a.s. 1"; horizontal and turned crosses, "a.s. 2" and "a.s. 3". Solid lines show the rhomb unit cell and the corresponding centered rectangle. (b) Circles, measured peak positions of the high-resolution x-ray diffraction pattern of Fig. 4. Dots, calculated $l=0$ diffraction peak positions for the five rotated domains (the cutoff is equal to $5\times10^{-4}$ with regard to peak "1" intensity calculated for one domain. Note that the interferences inside multicomponent peaks are not taken into account when superimposing the diffraction patterns of the five rotated approximant domains). (c) Calculated $l=1$ diffraction plane (the intensity cutoff with regard to the strongest peak in this picture is equal to $10^{-3}$). Spot radii are proportional to peak intensities. Pseudoextinction along axes 2' is verified.

of the quasicrystal [see Fig. 6(c)]; like the quasicrystal, the approximant exhibits (pseudo-)decagonal clusters. Calculated $l=0$ diffraction pattern of this approximant is shown in Fig. 14(b). It does not lead to an exact agreement with the experiment. Indeed, some weak measured peaks which were fitted with the nondecorated microcrystalline model are not generated for such a decoration within the cutoff interval of the calculation. On the contrary, some weak calculated peaks have not been measured. Such results could be attributed, for example, to the problem of the choice of the origin in hyperspace when generating the approximant: see Sec. V A. They must be partly due to the starting quasicrystal, since the quasicrystalline model already did not account for peaks of weak intensities (cf. Fig. 7). Nevertheless, despite these discrepancies, Fig. 14(b) clearly shows that for such a high-order approximant as the (5,7) one, a certain amount of calculated peaks present, as seen in Fig. 13, too weak intensities to be observed.

An important result concerning the pseudoextinction lines in the $l=1$ diffraction plane [Fig. 2(c)] must also be underlined. In their quasicrystalline models, Steurer and Kuo[14] and Burkov[25] introduced a screw axis and glide planes in hyperspace to account for the extinction of all the peaks belonging to axes 2'. When choosing for our microcrystalline unit cell a (5,7) approximant of one of their models, since the atomic arrangement in the unit cell still reflects rather well the atomic arrangement in the quasicrystal (roughly a 36° rotation from $z$ to $z+\frac{1}{2}$ planes), axes 2' are pseudoextinction lines, i.e., no relatively strong peaks are measurable on these axes. It is illustrated in Fig. 14(c) where an $l=1$ calculated diffraction pattern of a (5,7) approximant is drawn, clearly showing that there are no observable peaks located on axes 2' up to a low cutoff in intensity.

## V. DISCUSSION

### A. What approximant?

After showing that the unit cell in the microcrystalline $Al_{63}Cu_{17.5}Co_{17.5}Si_2$ is a (5.7) approximant, we have been faced with the question of its detailed atomic decoration, as discussed from Fig. 14(b). Within the scope of the cut-and-projection method, an extremely large number of approximants[59] can be calculated depending on the choice of the "origin" $\mathbf{Y}=(y_1,y_2,y_3,y_4,y_5)$. Moreover, linear transformation corresponding to small distortions may have to be applied after the cut operation to find the true structure of the approximant (it is not the object of the present work).

As mentioned in Sec. III B, there exists an infinity of equivalent Penrose-type quasicrytals corresponding to different origins $\mathbf{Y}=(y_1,y_2,y_3,y_4,y_5)$ with $\sum y_i=0$ and all their diffraction patterns are the same.[27] For crystalline approximants it is not the case, which is illustrated in Fig. 15: approximants of the same order (i.e., which have same unit-cell parameters), but calculated with different origins $\mathbf{Y}$, exhibit different diffraction patterns. For higher-order approximants, these differences mainly con-

cern peaks of weak intensities. At the present time, because our diffraction results are not quantitative enough and because the quasicrystalline model[14] does not account for weak intensity peaks, we have not been able to determine the **Y** origin. Moreover, even if the previous problems were solved, (5,7) approximants are so numerous that it would be difficult if not impossible to simulate all their diffraction patterns. In fact, other arguments such as energetic considerations[21,36,60,61] and crystallographic considerations[60(b)] about the unit-cell symmetries may be of a great help for the determination of the unit-cell atomic decoration.

One could also make a direct attempt to determine the unit-cell content. This unit cell ($a=b=51.5$ Å, $c=4.13$ Å, $\gamma=108°$) contains about 480 Al/Si atoms and 260 Cu/Co atoms (these numbers are computed for a density 4.7 g/cm$^3$). Its structure refinement could be performed for a single-domain sample. But for a microcrystalline sample, the direct attempt would probably fail because the composed peaks have to be rejected (see Sec. V C) and

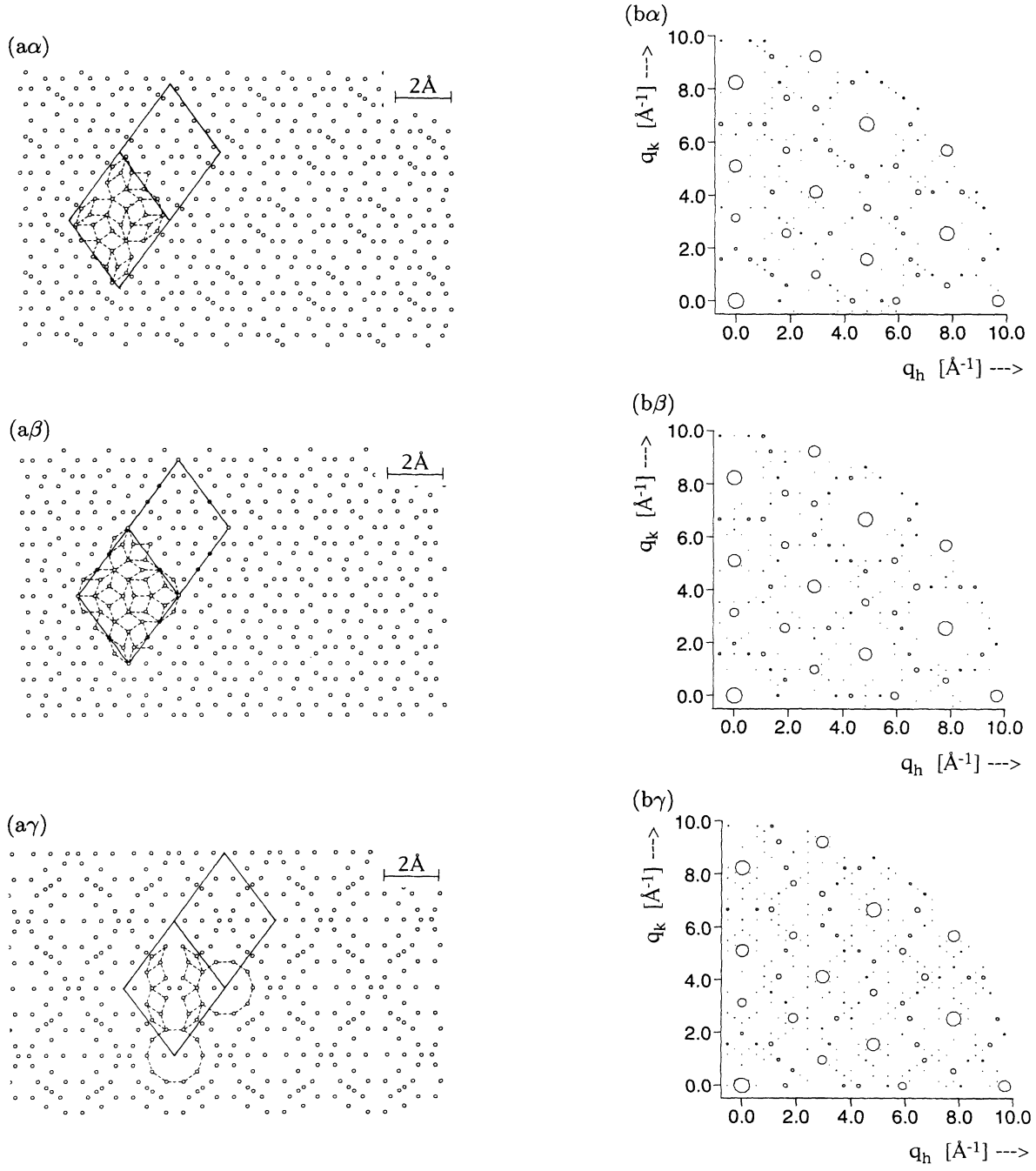


FIG. 15. (a) Direct space. Rhomb unit cells of (1,3) Penrose approximants (notation from Ref. 51) for different 5D origins: ($\alpha$) $\mathbf{Y}=\mathbf{Y}_0=(\frac{1}{3},-\frac{1}{7},\frac{1}{11},-\frac{1}{13},-\frac{614}{3003})$; ($\beta$) $\mathbf{Y}=(0.2236,-0.1412,0.4472,-0.3142,-0.2154)$; ($\gamma$) $\mathbf{Y}=(0,0,0,0,0)$. (b) Reciprocal space. Diffraction patterns corresponding to the approximants of (a) for an intensity cutoff $I/I(Q=0)$ equal to 0.01. Spot radii are proportional to intensities.

because a sufficient number of single peaks of reliable intensities could hardly be investigated. In brief, significant progress in this structure determination would be made if a single-domain sample was available.

### B. Domain arrangement in the microcrystal

In the microcrystalline state coherence lengths are probably larger than the domain sizes: coherence of the domains would be not only orientational but also positional. A direct proof of such a coherence has been found in icosahedral microcrystalline Al-Cu-Fe. Indeed, a high-resolution experiment has enabled the observation of separated components inside a strong multicomponent peak: see Fig. 3 in Ref. 62. In this figure, not all the components of the strong peak are found, which may be attributed to (destructive) interferences between some component peaks.[63]

Description of how the coherence can be maintained in a microcrystalline arrangement of domains is a difficult problem. A paradigm for the microcrystalline model would be a quasiperiodic arrangement of two types of domains with 36° and 72° rhombs if they present the rhombic forms of their unit cells.[46,64] In fact, one should rather consider that a microcrystal is formed of only one type of domain: it is almost certainly the case for microcrystalline Al-Cu-Fe (Ref. 49) and Al-Cu-Co-Si (Ref. 10 and Sec. IV B in this paper). If, for instance, one assumes that in decagonal planes the domains form sorts of large 72° rhombs, the problem of tiling a plane with 72° rhombs—which was raised by the quasicrystal discovery—is present at a larger scale. Then the coherence problem may lie for instance in the characteristics of the domain walls.[46,62,65,66] Further theoretical and experimental studies will be performed in order to try and understand this complicated problem.

### C. Consequence in structure determination if the sample considered as a quasicrystal is in fact a microcrystal

In this section, we will point out that the determination of a structure might be wrong if the sample supposed to be a quasicrystal is in fact a microcrystal and we will explain how to try and distinguish between a quasicrystal and a microcrystal by x-ray experiments. As shown above, domains are very probably arranged in a relatively coherent manner on a large scale in the microcrystal. Moreover, as explained in Sec. IV A, strong peaks in a microcrystal diffraction pattern are multicomponent ones. Under the assumption of domain coherence, the peaks inside such peaks interfere: there are interferences between peaks in exact coincidence and between overlapping wings of very close peaks. Let us consider only interferences between peaks in exact coincidence to illustrate consequence of interferences on structure determination in a simple manner. Let us take the very simple example of a microcrystal constructed from five domains formed of 72° rhombs and which have 72° orientational relationships [cf. Fig. 10(a)]. For such a simple model, interferences take place between peaks corresponding to diffracting planes parallel to the domain walls and they are constructive. So one finds two classes of composed peaks: (i) the ones in which there are no interferences: their intensities are roughly equal to the related quasicrystal peak intensities for a microcrystal formed of high order approximant domains; (ii) the ones in which there are interferences: their intensities are roughly equal to $\frac{1+1+1+4}{5}=\frac{7}{5}$ times the quasicrystal peak intensities. What we want to underline is as follows. If one wrongly takes a high-order single-domain approximant for a quasicrystal, structure determination within a quasicrystalline model will probably be valuable. But if one takes a microcrystal for a quasicrystal, due to the interference phenomena in multicomponent peaks which are just the strong ones, structure determination will surely be erroneous.

So, it is important to try—within experimental limitations—to distinguish between a quasicrystal and a microcrystal. Starting from x-ray diffraction patterns exhibiting quasicrystal-like characteristics, one can index diffraction peak positions not only in the scope of a quasicrystalline model but also in the scope of a microcrystalline model. If the microcrystalline model works, one can deduce from the crystalline unit cell the experimental conditions necessary to test the two models. For example, for icosahedral microcrystalline Al-Cu-Fe standard x-ray diffraction experiments are sufficient[49] whereas for decagonal microcrystalline Al-Cu-Co-Si "high-resolution" experiments are needed.

### D. On the proper determination of basis vectors in decagonal quasicrytals

Crystal diffraction patterns lead to an obvious determination of the basis vectors of the direct space lattice. As underlined in Refs. 3 and 18, it is not the case for quasicrystals because of the scaling property [illustrated in Fig. 11(c) by the pentagon sequence]. The possible parameters $d_s$ found for the hypercube are defined modulo $\tau^n$ (with $n$ integer) but it has no influence on the structure found after refinements.[3]

We will not point out another difficulty concerning the basis vector choice. We can illustrate it on our experimental data for microcrystalline Al-Cu-Co-Si. Indeed, in the following demonstration, only peaks of relatively strong intensities are used which should be in one-to-one correspondence with the strong intensity quasicrystalline peaks because the microcrystal unit cell is a high-order approximant of the quasicrystal. Depending on the wave-vector area where the diffraction pattern is obtained, two different sets of pentagon sequences can be chosen [see the solid and dotted line pentagons in Figs. 2(a), 3, and 4]. Solid line pentagons led to the basis chosen for the quasicrystal by SK.[14] If diffraction pattern had been available only in a small wave-vector area (Fig. 4), dotted line pentagons would have been chosen and new reciprocal basis vectors would have been determined, related to the first ones by an 18° rotation and a $1/\sqrt{(\tau+2)}$ factor (modulo $\tau^n$): the hyperspace parameter would have been found equal to $d_s\sqrt{(\tau+2)}$ (modulo $\tau^n$) instead of $d_s$. This result should be kept in mind when trying to elucidate the structure of decagonal quasicrystals.

Correlatively, let us mention (i) the discovery of a "de-

cagonal quasicrystal with superlattice ordering in Al-Ni-Co alloy" by Edagawa and co-workers.[67] Superlattice ordering is evidenced by the appearance of diffraction peaks of weak intensities which are indexed with new reciprocal basis vectors related to the parent lattice basis vectors just by an 18° rotation and a $1/\sqrt{(\tau+2)}$ factor (modulo $\tau^n$). Let us also mention (ii) the theoretical work of Lançon and co-workers who discuss "on choosing proper basis for determining structures of quasicrystals."[68] In the case of 2D tilings, they show how a wrong choice of the basis vectors, due to the nonobservation of weak superlattice peaks of the type of those of Ref. 67, can lead to important mistakes in the structure determination within the cut-and-projection formalism.

In the case of the present study and of the SK one, the $d_S=2.381$ Å value in hyperspace[14] and the $(r_0,72°)$ tile for the approximant in the microcrystalline state appear as the good choice. To prove it, let us assume that the choice of basis vectors is wrong for the decagonal quasicrystal of Ref. 14 or that the decagonal quasicrystal, to which the microcrystal approximant unit cell is related, is not the one described by SK but one in which superlattice ordering has occurred.[67] Then one would expect that use of a microcrystal formed of domains with a unit cell with a 72° angle and with edge $r_1=r_0[\sqrt{(\tau+2)}/\tau^2]$ $\approx 37.4$ Å or $r_1'=r_1\tau\approx 60.6$ Å, domain orientations differing from that used previously by an 18° rotation, would lead to the fitting of our experimental data. With such an assumption, only, respectively, 26 and 32 % of the measured peak positions in Fig. 4 are fitted, which demonstrates the above assertion about the proper choice of basis vectors in Al-Cu-Co-Si (similarly, for 36° domains, only 6 and 26 % of the measured peak positions are fitted).

## VI. CONCLUSION

We have presented single-crystal x-ray diffraction experiments performed on decagonal $Al_{63}Cu_{17.5}Co_{17.5}Si_2$. "High-resolution" experiments using synchrotron radiation are well interpreted within the scope of a microcrystalline model and not within that of a quasicrystalline model: the decagonal needles are in a microcrystalline state formed of crystalline domains having 72° orientational relationships, the unit cell of which can be described as a (5,7) approximant in the cut-and-projection formalism. Two questions remain open concerning the exact atomic decoration of this unit cell and the domain coherence.

The difficulties in structure determination for a microcrystal have been raised. They are mainly due to the absence of knowledge concerning both the domain arrangement and the nature of the domain walls. In particular, domain walls can modify peak intensities by introducing specific phase shifts. Very recently, high concentrations of vacancies have been found in quasicrystals.[69] If these results are confirmed, the location of the vacancies (domains, walls, etc.) will be an important parameter which will have to be introduced in the structure determination.

To conclude, we shall also consider our study in an energetical context. In Al-Cu-Co(-Si), the Hume-Rothery criterion (nesting of the pseudo-Brillouin zone defined from the strong diffraction peaks and of the Fermi surface) seems to be verified,[70] indicating that an electronic mechanism is to some extent responsible for the quasicrystal stability.[71] The Hume-Rothery criterion is also verified for the microcrystal because quasicrystal and microcrystal strong diffraction peaks are very close. In fact, although the Hume-Rothery mechanism plays an important role in the stabilization of quasicrystals, approximants,[72] and microcrystals, a more detailed description for their stability has still to be given. Transformations between quasicrystalline and microcrystalline states may be of a great help to get insights into the understanding of stability. Such transformations may take place in Al-Cu-Co(-Si) alloys.[73,60] After our careful structural analysis of the microcrystalline $Al_{63}Cu_{17.5}Co_{17.5}Si_2$, we plan to study the evolution of the samples versus temperature in order to investigate the possible occurrence of close states such as other microcrystalline approximants or the quasicrystalline state.

## ACKNOWLEDGMENTS

We are grateful to J. M. Godard for his very efficient assistance in the preparation of the ingot, to J. Doucet for providing us LURE facilities, and to D. Petermann for providing us computer facilities to collect our experimental data. It is also a pleasure to thank M. Baake, S. Burkov, G. Heger, M. Kalning, M. Kléman, F. Lançon, H. L. Li, W. Steurer, M. Widom, and R. Wittmann for fruitful discussions. Laboratoire de Physique des Solides is Unité de Recherche Associée au CNRS No. D0002.

[1]D. Shechtman, I. Blech, D. Gratias, and J. W. Cahn, Phys. Rev. Lett. **53**, 1951 (1984).

[2]L. Bendersky, Phys. Rev. Lett. **55**, 1461 (1985).

[3]W. Steurer, Z. Kristallogr. **190**, 180 (1990).

[4]L. X. He, Y. K. Wu, and K. H. Kuo, J. Mater. Sci. Lett. **7**, 1284 (1988).

[5]L. X. He, Y. K. Wu, X. M. Meng, and K. H. Kuo, Philos. Mag. Lett. **61**, 15 (1990).

[6]B. Grushko, Philos. Mag. Lett. **66**, 151 (1992); Phase Trans. **44**, 99 (1993).

[7]T. L. Daulton and K. F. Kelton, Philos. Mag. Lett. **63**, 257 (1991); T. L. Daulton, K. F. Kelton, S. Song, and R. Ryba, *ibid.* **65**, 55 (1992).

[8]S. Song, L. Wang, and E. R. Ryba, Philos. Mag. Lett. **63**, 335 (1991).

[9]P. Launois, M. Audier, F. Dénoyer, J. M. Godard, R. Reich, and M. Lambert, *Methods of Structural Analysis of Modulated Structures and Quasicrystals*, edited by J. M. Pérez-Mato, F. J. Zuniga and G. Madariaga (World Scientific, Singapore, 1991), pp. 545–554.

[10]M. Fettweis, P. Launois, F. Dénoyer, R. Reich, J. M. Godard, and M. Lambert, J. Non-Cryst. Solids **153&154**, 24 (1993).

[11]K. Hiraga, W. Sun, and F. J. Lincoln, Jpn. J. Appl. Phys. **30**, L302 (1991).
[12]X. Z. Liao, K. H. Kuo, H. Zhang, and K. Urban, Philos. Mag. B **66**, 549 (1992).
[13]L. X. He, X. Z. Li, Z. Zhang, and K. H. Kuo, Phys. Rev. Lett. **61**, 1116 (1988); Z. Zhang and K. Urban, Scr. Metall. **23**, 767 (1989); H. Zhang and K. H. Kuo, Phys. Rev. B **41**, 3482 (1990); L. X. He, T. Lograsso, and A. I. Goldman, *ibid.* **46**, 115 (1992).
[14](a) W. Steurer and K. H. Kuo, Acta Crystallogr. B **46**, 703 (1990); (b) Philos. Mag. Lett. **62**, 175 (1990).
[15]R. Reich *et al.* (unpublished).
[16]F. Frey and W. Steurer, J. Non-Cryst. Solids **153&154**, 600 (1993).
[17]M. Duneau and A. Katz, Phys. Rev. Lett. **54**, 2688 (1985).
[18]T. Janssen, Phys. Rep. **168**, 55 (1988).
[19]C. Janot, *Quasicrystals: A Primer* (Clarendon, Oxford, 1992), Chaps. 3 and 4.
[20]S. S. Kang and J. M. Dubois, J. Phys. Condens. Matter **4**, 10 169 (1992).
[21]C. L. Henley, J. Non-Cryst. Solids **153&154**, 172 (1993).
[22]C. L. Henley, in *Quasicrystals: The State of the Art,* edited by D. P. DiVincenzo and P. Steinhardt (World Scientific, Singapore, 1991), pp. 429–524.
[23]M. Widom, D. P. Cheng, and C. L. Henley, Phys. Rev. Lett. **63**, 310 (1989); K. J. Strandburg, Phys. Rev. B **40**, 6071 (1989); L. H. Tang and M. V. Jaric, *ibid.* **41**, 4524 (1990); S. E. Burkov, J. Phys. I (France) **2**, 695 (1992).
[24]S. E. Burkov, J. Stat. Phys. **65**, 395 (1991).
[25](a) S. E. Burkov, Phys. Rev. Lett. **67**, 614 (1991); (b) Phys. Rev. B **47**, 12 325 (1993).
[26]T. L. Daulton and K. F. Kelton, Philos. Mag. B **66**, 37 (1992).
[27]M. V. Jaric, Phys. Rev. B **34**, 4685 (1986).
[28]T. Janssen, Acta Crystallogr. A **42**, 261 (1986).
[29]K. N. Ishihara and A. Yamamoto, Acta Crystallogr. A **44**, 508 (1988).
[30]A. Pavlovitch and M. Kléman, J. Phys. A **20**, 687 (1987).
[31]We are working with the unitary projection matrices of, e.g., Refs. 27–29. Note that the W. Steurer and K. H. Kuo work is performed with another (equivalent) set of matrices (Refs. 3 and 14).
[32]Refined values concerning atomic surfaces are slightly different between Refs. 14(a) and 14(b). In particular, the "atom 3" Debye-Waller factor is equal to zero in Ref. 14(b). In the present paper, calculations are made from the results of Ref. 14(a) where the Debye-Waller factors of "atom 2" and "atom 3," both representing Al, are equal.
[33]K. Hiraga, in *Quasicrystals: The State of the Art,* edited by D. P. DiVincenzo and P. Steinhardt (World Scientific, Singapore, 1991), pp. 95–110.
[34]S. Kek (private communication), from W. Steurer, J. Non-Cryst. Solids **153&154**, 92 (1993).
[35]J. Dong, K. Lu, H. Yang, and Q. Shan, Philos. Mag. B **64**, 599 (1991).
[36]R. Phillips and M. Widom, J. Non-Cryst. Solids **153&154**, 416 (1993); R. Phillips, J. Zou, A. E. Carlsson, and M. Widom (unpublished).
[37]J. Roth, J. Stadler, R. Schilling, and H. R. Trebin, J. Non-Cryst. Solids **153&154**, 536 (1993).
[38]H. D. Carstanjen, R. M. Enrick, R. Grunwald, D. Plachke, and R. Wittmann, Phys. Rev. B **45**, 10 822 (1992).
[39]D. Plachke, T. Kupke, H. D. Carstanjen, and R. M. Emrick, J. Non-Cryst. Solids **153&154**, 72 (1993).
[40]W. Sigle, Philos. Mag. Lett. **68**, 39 (1993).
[41]Atomic structure factors used in our calculations are those determined from self-consistent or variational wave functions in the *International Tables for Crystallography,* Tome III (Kynoch, Birmingham, 1962). We checked our calculation programs by comparing the structure factors we calculated with the ones Steurer and Kuo calculated in their list of structure factors (available upon request [Ref. 14(a)]).
[42]L. Pauling, Nature **317**, 512 (1985).
[43]R. D. Field and H. L. Fraser, Mater. Sci. Eng. **68**, L17 (1984); W. J. Jiang, Z. K. Hei, Y. X. Guo, and K. H. Kuo, Philos. Mag. A **52**, L53 (1985); K. K. Fung, X. Zou and C. Y. Yang, Philos. Mag. Lett. **55**, 27 (1987).
[44]G. Friedel, *Leçons de Cristallographie* (Libraire, Scientifique Albert Blanchard, Paris, 1921); R. K. Mandal, S. Lele, and S. Ranganathan, Philos. Mag. Lett. **67**, 301 (1993).
[45]J. Wolny, L. Pytlik, and B. Lebech, J. Phys. C **21**, 2267 (1988).
[46]M. Lambert and F. Dénoyer, C. R. Acad. Sci. Paris **309**, 1463 (1989).
[47]T. L. Ho and Y. H. Li, Phys. Rev. Lett. **62**, 917 (1989).
[48]P. Launois, M. Audier, F. Dénoyer, C. Dong, J. M. Dubois, and M. Lambert, Europhys. Lett. **13**, 629 (1990); **14**, 283 (1991).
[49]F. Dénoyer, G. Heger, M. Lambert, M. Audier, and P. Guyot, J. Phys. (Paris) **51**, 651 (1990); T. Motsch, F. Dénoyer, P. Launois, and M. Lambert, J. Phys. I (France) **2**, 861 (1992).
[50]A. I. Goldman and K. F. Kelton, Rev. Mod. Phys. **65**, 213 (1993); **65**, 579 (1993).
[51]K. Edagawa, K. Suzuki, M. Ichihara, and S. Takeuchi, Philos. Mag. B **64**, 629 (1991).
[52]D. Paquet, M. C. Joncour, F. Mollot, and B. Etienne, Phys. Rev. B **39**, 10 973 (1989).
[53]V. E. Dmitrienko, J. Phys. France **51**, 2717 (1990), see Fig. 2.
[54]Note also that recently M. Kalning, S. Kek, B. Burandt, W. Press, and W. Steurer found, with the use of x-ray diffraction technique and studying a multicomponent peak, a microcrystalline state in $Al_{70}Ni_{15}Co_{15}$, the domain unit cell being a rhomb with edge $r_0' = 51.91$ Å and with acute angle $\alpha \approx 72°$ (unpublished).
[55]In previous studies, with an alloy of nominal composition (63/17, 5/17, 5/2) but prepared differently [by C. Dong and J. M. Dubois (unpublished)], we also found that fitting of the data obtained performing x-ray diffraction experiments of standard resolution was possible with 36° rhombs with edges $r_0$ and $r_0/\tau$ ($r_0 = 51.5$ Å) and 72° rhombs with edges $r_0$ and $r_0/\tau$ (Ref. 48). Nevertheless, high-resolution electron microscopy observation of the 36° rhomb with edge length $r_0$ was put forward. Although high-resolution electron microscopy gives important local information about the structure as underlined, for example, by K. Hiraga (Ref. 33), the spatial limitation of the experiment must be taken into account when interpreting the data. Different high-resolution electron microscopy patterns have now been seen for our first samples (see Fig. 2 in Ref. 48 and Fig. 9 in Ref. 56) and electron diffraction data (Ref. 57) were fitted with the 72° rhomb with edge length $r_0$ [like high-resolution x-ray experiments for our present samples (Ref. 10)]. Hence we are no more confident in the fact that the $(r_0, 36°)$ rhomb may be representative of the bulk structure of our first samples: they may have been in the same microcrystalline state as our present samples.
[56]C. Dong, J. M. Dubois, S. S. Kang, and M. Audier, Philos. Mag. B **65**, 107 (1992).
[57]M. Audier, P. Launois, F. Dénoyer, M. Lambert, C. Dong, and J. M. Dubois, Microsc. Microanal. Microstruct. **1**, 417 (1990).

[58]H. Zhang and K. H. Kuo, Phys. Rev. B **42**, 8907 (1990).
[59]M. Widom (private communication).
[60](a) M. Widom and R. Phillips, J. Non-Cryst. Solids **153&154**, 282 (1993). (b) E. Cockayne, R. Phillips, X. B. Xan, S. C. Moss, J. L. Robertson, T. Ishimasa, and M. Mori, J. Non-Cryst. Solids **153&154**, 140 (1993).
[61]M. Krajci and J. Hafner, Phys. Rev. B **46**, 10 669 (1992).
[62]F. Dénoyer, P. Launois, T. Motsch, and M. Lambert, J. Non-Cryst. Solids **153&154**, 595 (1993).
[63]F. Dénoyer *et al.* (unpublished).
[64]R. Mosseri, J. Non-Cryst. Solids **153&154**, 658 (1993).
[65]G. Coddens, J. Phys. I (France) **1**, 523 (1991).
[66]M. Duneau, J. Phys. I (France) **1**, 1591 (1991).
[67]K. Edagawa, M. Ichihara, K. Suzuki, and S. Takeuchi, Philos. Mag. Lett. **66**, 19 (1992).
[68]F. Lançon, L. Billard, S. Burkov, and M. de Boissieu, J. Phys. I (France) **4**, 283 (1994).
[69]S. S. Kang and J. M. Dubois, Philos. Mag. A **66**, 151 (1992); R. Chidambaran, M. K. Sanyal, V. S. Raghunathan, P. M. G. Nambissan, and P. Sen, Phys. Rev. B **48**, 3030 (1993).
[70]A. P. Tsai, A. Inoue, and T. Masumoto, Mater. Trans., JIM **30**, 463 (1989).
[71]H. Friedel and F. Dénoyer, C. R. Acad. Sci. Paris **305**, 171 (1987).
[72]F. Hippert, L. Kandel, Y. Calvayrac, and B. Dubost, Phys. Rev. Lett. **69**, 2086 (1992).
[73](a) C. Dong, J. M. Dubois, M. de Boissieu, and C. Janot, J. Phys.: Condens. Matter **3**, 1665 (1991); (b) B. Grushko, R. Wittmann, and K. Urban, J. Mater. Res. **7**, 2713 (1992). A microcrystal-quasicrystal transformation is reported in (a), it is discussed with regards to the melting of an intergrain phase in (b). (c) G. Coddens and P. Launois, J. Phys. I (France) **1**, 993 (1991); P. Launois and G. Coddens, in *Methods of Structural Analysis of Modulated Structures and Quasicrystals,* edited by J. M. Pérez-Mato, F. J. Zuniga, and G. Madariaga (World Scientific, Singapore, 1991), pp. 634–636; S. S. Song and E. R. Ryba, Philos. Mag. Lett. **65**, 85 (1992).

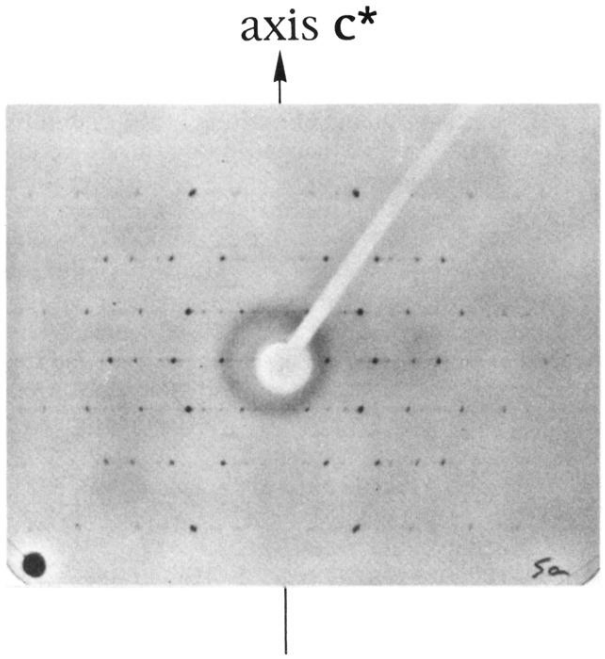


FIG. 1. Monochromatic rotating crystal pattern of decagonal $Al_{63}Cu_{17.5}Co_{17.5}Si_2$: $\lambda = 0.711$ Å (Mo $K\alpha$ radiation), the wavelength is selected using the (0,0,2) reflection of a pyrolytic graphite monochromator, $\lambda/n$ ($n = 2,3$) contaminations are avoided by choosing adequate generator voltage. The needle axis is parallel to the pattern.

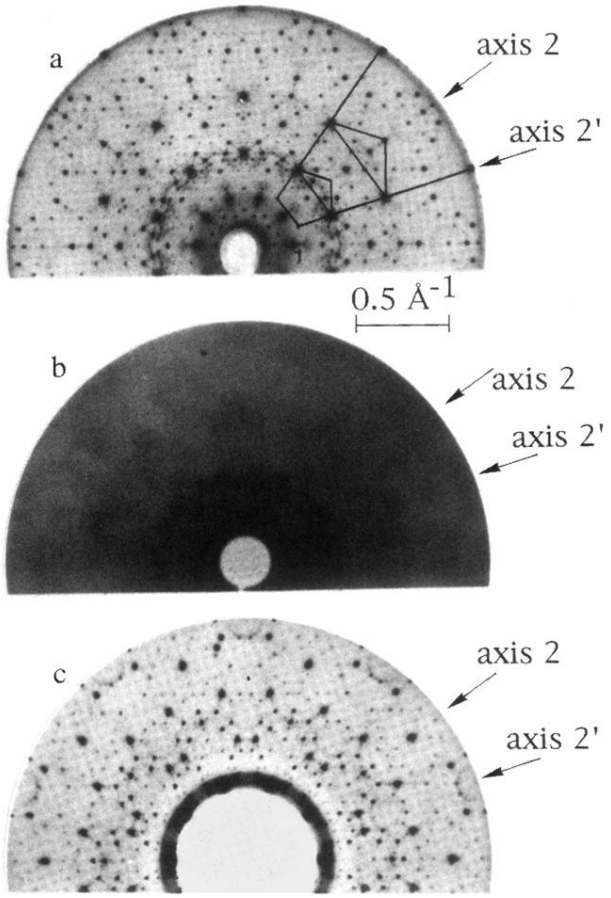


FIG. 2. Monochromatic x-ray precession patterns of decagonal $Al_{63}Cu_{17.5}Co_{17.5}Si_2$ obtained using Mo $K\alpha$ radiation ($\lambda$=0.711 Å), the wavelength is selected using the (0,0,2) reflection of a pyrolytic graphite monochromator, $\lambda/n$ ($n=2,3$) contaminations are avoided by choosing adequate generator voltage. (a) $l=0$ reciprocal plane (zero level reciprocal plane perpendicular to the periodic axis $\mathbf{c}^*$). The sample-film distance is 60 mm. We refer to solid and dotted line pentagons in Sec. V. (b) $l=\frac{1}{2}$ reciprocal plane: diffuse scattering. (c) $l=1$ reciprocal plane: note the pseudoextinction observed along one of the two types of twofold axes (termed 2'). Scales are indicated in the picture: in this paper, all reciprocal vectors are defined without $2\pi$ factor.

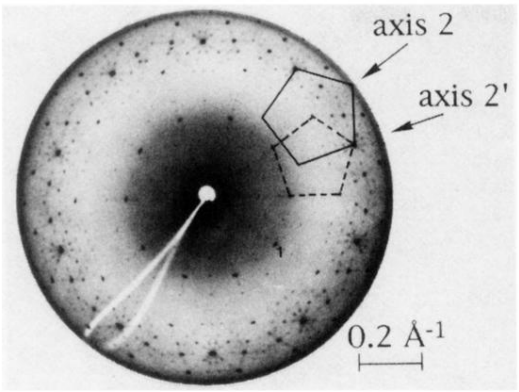


FIG. 3. Monochromatic x-ray precession pattern obtained from the $l=0$ reciprocal plane perpendicular to the periodic axis $\mathbf{c}^*$ using Cu $K\alpha$ radiation [$\lambda=1.542$ Å, the wavelength is selected using the (0,0,2) reflection of a pyrolytic graphite monochromator, some very weak reflections may be due to small contaminations by $\lambda/2$ or $\lambda/3$ radiations; the sample-film distance is 60 mm].

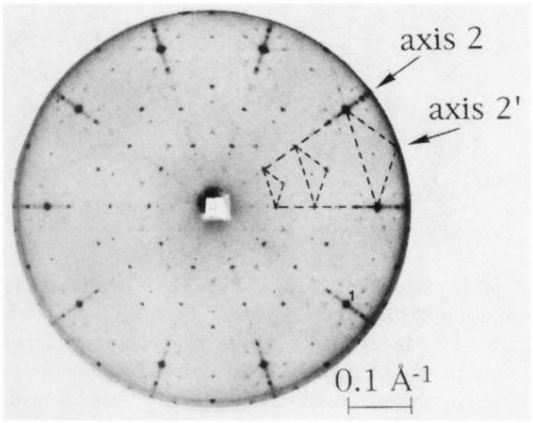


FIG. 4. Monochromatic x-ray precession pattern obtained from the $l=0$ reciprocal plane perpendicular to the periodic axis $\mathbf{c}^*$. The x-ray wavelength $\lambda=1.495$ Å is selected using the (1,1,1) reflection of a germanium monochromator (no $\lambda/2$ contamination). The sample-film distance is 125 mm and beam collimation is better than for experiments with standard x-ray sources. This pattern obtained with synchrotron radiation is a better resolution one. Spots 1 have the strongest intensity.